Article

SOURCE DATA OPEN ACCESS

THE EMBO JOURNAL

m^6A RNA methyltransferases METTL3/14 regulate immune responses to anti-PD-1 therapy

Lingling Wang[1], Hui Hui[1,2], Kriti Agrawal[1,2], Yuqi Kang[1,2], Na Li[1], Rachel Tang[1], Jiajun Yuan[1] & Tariq M Rana[1,3,*]

Abstract

An impressive clinical success has been observed in treating a variety of cancers using immunotherapy with programmed cell death-1 (PD-1) checkpoint blockade. However, limited response in most patients treated with anti-PD-1 antibodies remains a challenge, requiring better understanding of molecular mechanisms limiting immunotherapy. In colorectal cancer (CRC) resistant to immunotherapy, mismatch-repair-proficient or microsatellite instability-low (pMMR-MSI-L) tumors have low mutation burden and constitute ~85% of patients. Here, we show that inhibition of *N*^{6}-methyladenosine (m^6A) mRNA modification by depletion of methyltransferases, Mettl3 and Mettl14, enhanced response to anti-PD-1 treatment in pMMR-MSI-L CRC and melanoma. Mettl3- or Mettl14-deficient tumors increased cytotoxic tumor-infiltrating CD8$^+$ T cells and elevated secretion of IFN-γ, Cxcl9, and Cxcl10 in tumor microenvironment *in vivo*. Mechanistically, Mettl3 or Mettl14 loss promoted IFN-γ-Stat1-Irf1 signaling through stabilizing the *Stat1* and *Irf1* mRNA via Ythdf2. Finally, we found a negative correlation between METTL3 or METTL14 and STAT1 in 59 patients with pMMR-MSI-L CRC tumors. Altogether, our findings uncover a new awareness of the function of RNA methylation in adaptive immunity and provide METTL3 and METTL14 as potential therapeutic targets in anticancer immunotherapy.

Keywords CD8$^+$ T cells; colorectal carcinoma; immunotherapy; m^6A methylation

Subject Categories Immunology; RNA Biology

DOI 10.15252/embj.2020104514 | Received 19 January 2020 | Revised 29 July 2020 | Accepted 7 August 2020 | Published online 23 September 2020

The EMBO Journal (2020) 39: e104514

Introduction

Immunotherapy has become one of the unprecedented treatment modalities for multiple cancers by targeting the interactions between tumor and immune system (Ribas & Wolchok, 2018). The immune system discriminates exogeneous cells from self through the recognition of the major histocompatibility complex (MHC) complex-peptides presented on target cells, e.g., tumor cell, and T cell receptors (TCR) on immune cells (Schreiber *et al*, 2011; Khalil *et al*, 2016), whereas this recognition alone is not sufficient for initiation of the immune response. Other regulatory circuits also play important roles to co-inhibit or co-activate immune cells, the former role is typically exploited by cancer cells to evade immunosurveillance (Townsend & Allison, 1993; Sharma & Allison, 2015; Wei *et al*, 2018b). Among these negative regulatory pathways, PD-1 (programmed cell death–1) and CTLA-4 (cytotoxic T-lymphocyte protein 4) have been targeted by immune checkpoint inhibitors (ICIs) to enhance tumor cell killing by T cells in immunotherapy (Jenkins *et al*, 2018). Tumors with mutated genome are likely to generate peptide neoantigen to recruit and activate immune cells via MHC complex-TCR recognition in immunotherapy to induce durable response (Samstein *et al*, 2019). Although impressive success has been observed in the clinical practice of ICIs for tumors with high mutation burden, such as non-small cell lung cancer (NSCLC) and melanoma, while the failure of response or elapse in low-mutation-burden cancer patients treated with ICIs remains common (Alexandrov *et al*, 2013; Sharma *et al*, 2017; Ganesh *et al*, 2019). In addition to mutational load, a number of other useful biomarkers for ICI responses have been identified including interferon signatures (Ayers *et al*, 2017), checkpoint ligand expression, and inflammation in tumor microenvironments (Kowanetz *et al*, 2018).

Mismatch-repair deficiency or high level of microsatellite instability (dMMR-MSI-H) in tumors has emerged as an effective biomarker to predict solid tumor responses to ICIs (Le *et al*, 2017; Mandal *et al*, 2019). dMMR-MSI-H tumors possess microsatellite instability (MSI) leading to genetic hypermutability and accumulation of thousands of mutations. These studies are exciting and provide a proof of concept that reliable biomarkers could provide important criteria for patient stratification for ICI therapies. However, mismatch-repair-proficient or microsatellite instability-low (pMMR-MSI-L) tumors have low mutation burden and constitute ~85% of CRC patients (Ganesh *et al*, 2019). Apart from the status of mutation burden, lack of response or being resistant to ICIs also involves the alternations of molecular mechanisms in both cancer and immune system as well as their interface (Sharma *et al*, 2017). Within these alternations, the abnormality of T cells, the

1 Division of Genetics, Department of Pediatrics, Program in Immunology, Institute for Genomic Medicine, University of California San Diego, La Jolla, CA, USA
2 Bioinformatics Program, University of California San Diego, La Jolla, CA, USA
3 San Diego Center for Precision Immunotherapy, Moores Cancer Center, University of California San Diego, La Jolla, CA, USA
*Corresponding author. Tel: +1 858 246 1100; E-mail: trana@ucsd.edu

absence of antigen presentation, and the aberrant oncogenic signaling were revealed by recent studies (Sharma *et al*, 2017). Therefore, new mechanisms governing the response and resistance to ICIs therapy need to be discovered. In addition, mechanism-driven biomarkers should be identified for guiding cancer immunotherapy for pMMR-MSI-L tumors in CRC.

N^6-methyladenosine (m^6A) is the most abundant chemical modification in mRNA and lncRNA in eukaryotes (Dominissini *et al*, 2012; Meyer *et al*, 2012; Yue *et al*, 2015; Meyer & Jaffrey, 2017). In mammalian cells, this epitranscriptomic mark is installed by methyltransferase machinery comprising a METTL3-METTL14 core and other subunits (Liu *et al*, 2014; Ping *et al*, 2014). The reversal of this modification is mediated by the alpha-ketoglutarate-dependent dioxygenases FTO and ALKBH5 (Jia *et al*, 2011; Zheng *et al*, 2013). Dynamics of RNA methylation influences a broad range of physiological processes including RNA metabolism and protein translation mainly through the readout of YTH family m^6A binding proteins (Wang *et al*, 2014, 2015; Xiao *et al*, 2016; Hsu *et al*, 2017; Li *et al*, 2017; Nachtergaele & He, 2018). Aberrant m^6A RNA methylation is associated with various diseases including cancer (Deng *et al*, 2018; Wu *et al*, 2019). Recently, studies have started to provide emerging roles of RNA methylation and its machinery in tumor initiation, differentiation, and progression (Jaffrey & Kharas, 2017; Liu *et al*, 2019). Moreover, elevation of RNA methylation affects both immune response and melanoma cell sensitivity within anticancer immunotherapy (Han *et al*, 2019; Yang *et al*, 2019). Despite this discovery, suppression of m^6A had also been observed in the tumorigenesis (Deng *et al*, 2018). Recently, depletion of ALKBH5 in sensitizing tumors to cancer immunotherapy has been described where ALKBH5 modulates target gene expression and splicing, leading to changes in lactate content of the tumor microenvironment, which regulates the composition of tumor-infiltrating Treg and myeloid-derived suppressor cells (Li *et al*, 2020). Remarkably, a small-molecule inhibitor of ALKBH5 enhanced the efficacy of cancer immunotherapy (Li *et al*, 2020). The complex and varied roles of m^6A in tumors suggest that much needs to be done to further understand the importance and dynamic of this modification in cancer biology and its clinical application. Besides, apart from total mutation burden, whether RNA methylation pathway involves the insensitivity of refractory cancer in immunotherapy remains unknown.

Here, we present that the disruption of m^6A methyltransferases enhanced immunotherapy response in pMMR-MSI-L colorectal cancer through modulating the intratumor microenvironment and tumor-infiltrating cells. Mechanistically, depletion of Mettl3 or Mettl14 enhanced IFN-γ-Stat1-Irf1 signaling through stabilizing the *Stat1* and *Irf1* mRNA mediated by Ythdf2. Our findings uncovered, a previously unrecognized, mechanism of mRNA methylation in sensitizing pMMR-MSI-L colorectal cancer to PD-1 blockade, thereby providing potential new biomarkers and a therapeutic avenue for this malignant disease refractory to ICIs treatment.

Results

Loss of Mettl3 or Mettl14 sensitizes colorectal carcinoma and melanoma tumors to anti-PD-1 treatment

So far, the roles of m^6A methyltransferases (METTL3 and METTL14) in cancer immunotherapy have not been investigated. To determine the biological function of METTL3 and METTL14 in this process, we employed mouse models using the modestly immunogenic colorectal cancer cell line CT26 (Kim *et al*, 2014) and a poorly immunogenic murine melanoma cell line B16 (Manguso *et al*, 2017). Loss of Mettl3 and Mettl14 CT26 colorectal carcinoma and B16 melanoma cells were generated using sgRNA and validated the effect of depletion by Western blotting (Fig 1A and B). To establish these mouse models, we first investigated the immune checkpoint-blocking antibody response in CT26 tumors. We treated BALB/c mice bearing CT26 colorectal carcinoma with control IgG, anti-PD-1, or combined anti-PD-1 plus anti-CTLA-4 antibodies. Anti-PD-1 antibody had limited effect on tumor growth and mice survival compared with control IgG antibody treatment, whereas combined anti-PD-1 and anti-CTLA-4 treatment responded better than anti-PD-1 (Fig EV1A and B), consistent with the previous study (Kim *et al*, 2014) showing resistance to anti-PD-1 treatment in colon cancer immunotherapy. Next, Mettl3- or Mettl14-depleted and control cells were subcutaneously injected into BALB/c mice, and mice were treated with anti-PD-1 antibody. Compared to control, the mice bearing Mettl3- or Mettl14-depleted CT26 tumors showed slower tumor growth (Figs 1C and EV1C) and prolonged survival (Fig 1E). We also analyzed the effect of Mettl3 or Mettl14 depletion in a well-established B16 melanoma model where C57BL/6J mice were treated with combination of anti-PD-1 antibody and granulocyte-macrophage colony-stimulating factor (GM-CSF)-secreting irradiated B16 cell vaccine (GVAX), which simulates an adaptive immune response (Manguso *et al*, 2017). Consistent with the results of CT26, Mettl3- or Mettl14-deficient-B16-tumor-bearing mice exhibited tumor growth inhibition (Figs 1D and EV1D) and longer survival than controls (Fig 1F). Additionally, we confirmed that Mettl3 and Mettl14 were efficiently repressed in these mouse tumors by Western blot (Fig EV1E and F) and found the expression of Ki-67 was decreased in Mettl3- or Mettl14-depleted tumors using immunohistochemistry (IHC) staining, which indicated that Mettl3 or Mettl14 null tumors were smaller than control tumors caused reduced proliferation (Fig EV1G). Then, we assessed whether Mettl3 or Mettl14 depletion alone was able to affect cell or tumor growth since Mettl3 and Mettl14 are lethal in particular cancer types such as leukemia (Barbieri *et al*, 2017; Vu *et al*, 2017; Weng *et al*, 2018), glioblastoma (Cui *et al*, 2017), and hepatocellular carcinoma (Ma *et al*, 2017; Chen *et al*, 2018). Our observation revealed that all the cells and tumors with control and Mettl3 or Mettl14 knockout have quite similar cellular proliferation *in vitro* (Fig EV2A) and tumor volume *in vivo* (Fig EV2B–E). Collectively, these results suggested a generalizable role of m^6A methyltransferases in colorectal carcinoma and melanoma, where the loss of Mettl3 or Mettl14 sensitizes tumor to the effect of immunotherapy, but not intrinsically impairs their growth alone.

Depletion of Mettl3 or Mettl14 increased cytotoxic tumor-infiltrating $CD8^+$ T cells and altered tumor microenvironment

To identify the mechanisms by which depletion of Mettl3 or Mettl14 increased the response to immunotherapy, we analyzed the immune cell components within the CT26 tumor tissues by flow cytometry. The immune infiltrates contained significantly increased $CD8^+$ T cells in both Mettl3 and Mettl14 null tumors compared to control tumors (Figs 2A and EV3A), whereas no

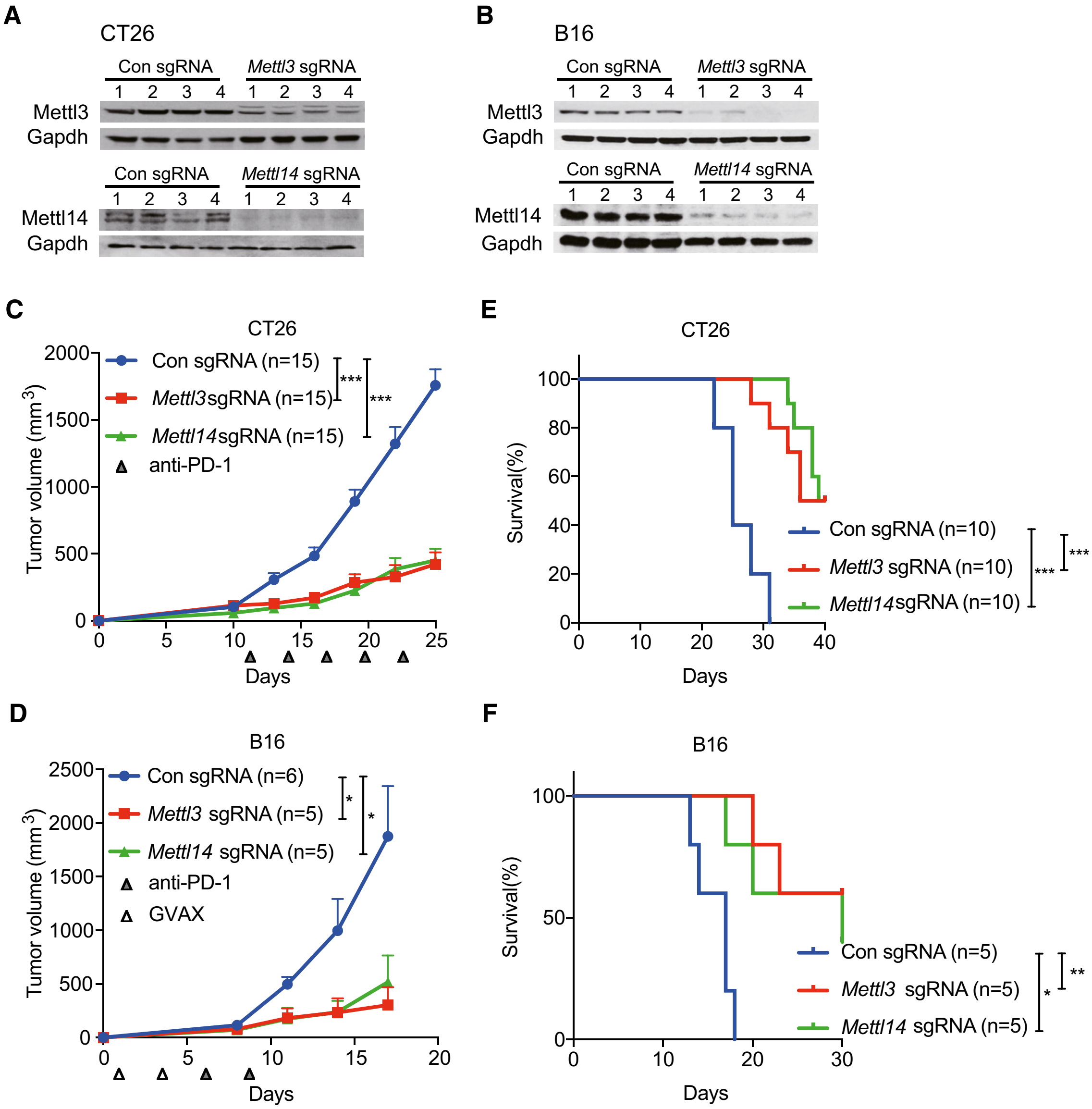

Figure 1. Depletion of Mettl3 or Mettl14 sensitizes CT26 and B16 tumors to immunotherapy.

A, B Immunoblotting were performed to validate Mettl3 or Mettl14 expression levels in CT26 and B16 cells as indicated. Gapdh served as a loading control.

C, D Tumor volume was monitored for control and Mettl3- or Mettl14-depleted tumors with treatment as indicated in CT26 colon cancer and B16 melanoma, respectively. Data are mean ± SEM of the indicated number of mice in each group. *n*, the numbers of mice. *$P < 0.05$; ***$P < 0.001$ by Student's *t*-tests.

E, F Survival analysis of control tumors and those with depleted genes were recorded as indicated in CT26 colon cancer and B16 melanoma, respectively. Data are mean ± SEM of the indicated number of mice in each group. *n*, the numbers of mice. *$P < 0.05$; **$P < 0.01$; ***$P < 0.001$ by Student's *t*-tests.

Source data are available online for this figure.

differences in the $CD4^+$ T cells, $CD45^+$ cells, and Treg cells were observed (Fig 2A). Additionally, the level of natural killer (NK) cells is higher from Mettl14-deficient tumors than that of control tumors (Fig 2A). In line with the observations of flow cytometry analysis, we also found that Mettl3- and Mettl14-depleted tumors had higher expression of CD8 than that of control (Fig 2B). Further analysis revealed that Mettl3- and Mettl14-depleted tumors contained a dramatically enhanced granzyme B expression in $CD8^+$ T cells (Fig 2C). Consistently, compared with control tumors, we observed increased $CD8^+$ T cells and granzyme B expression in $CD8^+$ T cells from Mettl3 and Mettl14 null B16 tumors as well (Fig EV3B and C). Taken together, loss of Mettl3 or Mettl14 improved cytotoxic tumor-infiltrating $CD8^+$ T cells. To further investigate the contributions of $CD8^+$ T cells to the antitumor response of immunotherapy, we depleted $CD8^+$ T cells using an anti-CD8 antibody and monitored the tumor growth from mice bearing control, Mettl3, or Mettl14 null tumors during immunotherapy. Our results showed that enhanced response to immunotherapy caused by depletion of Mettl3 or Mettl14 was completely abolished in both CT26 and B16 tumors (Fig 2D and

E), indicating that $CD8^+$ T cells are essential for controlling tumor growth (Ribas & Wolchok, 2018).

$CD8^+$ T cells are multiple cytokine producers (Paliard *et al*, 1988), which predominately secrete cytokines including IFN-γ and TNFα (Lichterfeld *et al*, 2004; Pandiyan *et al*, 2007). IFN-γ plays an important role in tumor immune surveillance (Castro *et al*, 2018) via inducing the production of CXCL9 and CXCL10, where these chemokines facilitate recruitment of $CD8^+$ and $CD4^+$ effector T cells to suppress tumor growth (Gorbachev *et al*, 2007; Tokunaga *et al*, 2018). To address this question, we then analyzed the secretion of IFN-γ, Cxcl9, and Cxcl10 in both mouse serum and intratumor using ELISA. Our results showed that the production of IFN-γ and Cxcl10 was not significantly changed in mouse serum (Figs 2F and EV3F) except for Cxcl9 (Fig EV3D). Interestingly, we observed a remarkably increased concentration of IFN-γ (Fig 2G), Cxcl9 (Fig EV3E), and Cxcl10 (Fig EV3G) in both Mettl3- and Mettl14-deficient intratumor relative to control intratumor. Together, these results indicate a mechanism where Mettl3 or Mettl14 loss enhanced efficacy of immunotherapy through modulating production of cytokines and chemokines in the tumor microenvironment.

Identification of potential targets of Mettl3 and Mettl14

To understand the molecular mechanism of Mettl3 and Mettl14 in cancer immunotherapy, we employed RNA sequencing (RNA-seq) to identify the affected genes upon Mettl3 and Mettl14 depletion. Through analysis of our RNA-seq data, we identified the mRNA transcript level of 402 genes was upregulated and 282 genes was downregulated in Mettl3 null tumors compared to control tumors, while 283 genes were increased and 73 genes were decreased in Mettl14-deficient tumors compared with control (Fig 3A). Furthermore, 230 Mettl3- and Mettl14-dependent genes were altered among both tumors with knockout of Mettl3 and Mettl14 compared to control: including 202 co-upregulated and 28 co-downregulated genes (Fig 3B, Dataset EV1). Gene ontology (GO) analysis was performed on 202 co-upregulated genes since the limited numbers of co-downregulated genes, and these enriched pathways were mainly associated with responses to interferons, defense, inflammation, leukocyte cell–cell adhesion, cytokine production, adaptive immunity, and antigen processing and presentation (Fig 3C). Notably, Mettl3- and Mettl14-dependent upregulated genes involved in interferon-gamma and interferon-beta pathways including *Stat1*, *Stat4*, *Irf1*, *Irf4*, *Irf7,* and *Pdl1*, and cytokine/chemokine-mediated signaling pathway such as *Ccl5*, *Cxcl9,* and *Cxcl10*, which was consistent with our previous observation of productions of chemokines (Fig EV3E and G). To validate our RNA-seq results, we performed qRT–PCR and our results showed that all of these genes involved in interferons and cytokine/chemokine pathways were significantly upregulated in Mettl3 and Mettl14 null tumors (Fig EV4A). Together, these findings suggested that the upregulated genes upon Mettl3 and Mettl14 depletion were principally connected with immune response-associated processes.

We then asked whether the altered gene expression caused by Mettl3 and Mettl14 depletion was a consequence of suppressed m^6A methylation. We first analyzed the total m^6A modification levels by dot-blot experiments, which were significantly decreased in the Mettl3 and Mettl14 null tumors compared with control tumors (Fig EV4B). Next, m^6A methylome between control and methyltransferase-depleted tumors were compared by antibody-based m^6A immunoprecipitation together with high-throughput sequencing (MeRIP-seq) as described previously (Lichinchi *et al*, 2016a,b; Lichinchi & Rana, 2019). In line with total methylation level changes on mRNA, after combining the peaks in replicates, our analysis identified 16,883 high-confidence m^6A peaks in control tumor, whereas 7,701 and 8,794 m^6A peaks were identified in Mettl3- and Mettl14-deficient tumors, respectively (Fig EV4C). These results indicate a global loss of m^6A methylation in methyltransferase-depleted tumors. To investigate the role of m^6A on the regulation of mRNA level, we identified the upregulated, downregulated, and unchanged m^6A-containing genes from MeRIP-seq and RNA-seq data. Although the majority of m^6A-containing genes (6,728) were unchanged, 64 m^6A-containing genes were co-upregulated in both Mettl3- and Mettl14-deficient tumors, whereas only 12 m^6A-containing genes were downregulated, which reflected the specific regulatory role of m^6A in response to immunotherapy and indicated the destabilization effect of m^6A modification on RNA (Fig EV4D). Then, GO analysis was performed on 64 co-upregulated m^6A-containing genes, and these enriched pathways were also related to immune response, predominately associated with response to interferons, regulation of cytokine production, adaptive immune response, and defense response, etc. (Fig EV4E, Dataset EV2). Furthermore, depletion of Mettl3 and Mettl14 decreased m^6A enrichment in 3′UTR where the majority of m^6A control the stability of mRNA, mirrored the upregulated overall genes and m^6A-containing genes (Fig EV4F and G). Moreover, previously identified GGACU m^6A consensus motif was highly enriched within m^6A peaks in the control tumors (Fig 3D).

To identify the potential targets of Mettl3 and Mettl14, we developed a workflow scheme outlined in Fig 3E. We filtered 202 co-upregulated genes enriched in pathways that were found in the RNA-seq with 11,167 m^6A peaks which were lost in both Mettl3 and Mettl14 null tumors. This analysis resulted in 55 candidate genes identification including *Stat1* and *Irf1* (Fig 3E, Dataset EV3). Given that STAT1 and IRF1 not only act as fundamental role in Janus kinase (JAK)–STAT signaling, which is involved in antiviral and antibacterial response (Ramana *et al*, 2000; Honda *et al*, 2006; Pautz *et al*, 2010), but also play a critical role in IFN-γ signaling (Sharma *et al*, 2017) and anti-PD-1 response (Garcia-Diaz *et al*, 2017; Zenke *et al*, 2018), which results in antitumor effects. Then, we further analyzed our MeRIP-seq data, which showed that Mettl3 and Mettl14 deposit m^6A on 3′UTR (near stop codon) of both *Stat1* and *Irf1*, and these two m^6A sites have drastically decreased methylation level in Mettl3 and Mettl14 null tumors (Fig 3F). We further validated these findings by MeRIP-qPCR showing significant decrease in *Stat1* and *Irf1* mRNA levels in Mettl3 and Mettl14 null tumors demonstrating that our MeRIP-seq data were robust and accurate (Fig 3G). In agreement with the transcript level of *Stat1* and *Irf1* validated by qRT–PCR (Fig EV4A), we also observed an increased Stat1, phosphorylated (p-) Stat1 and Irf1 protein levels in the Mettl3 and Mettl14 null tumors (Fig 3H). To further investigate whether the mechanism of enhanced immunotherapy response of Mettl3 or Mettl14 null tumors relies on the increased Stat1 and Irf1, we generated knockout of Stat1 or Irf1 CT26 cells based on the Mettl3- or Mettl14-depleted cells we already had, and then double knockout of Mettl3/Stat1, Mettl3/Irf1, Mettl14/Stat1, or Mettl14/Irf1 CT26 cells were obtained and validated the effect via Western blot

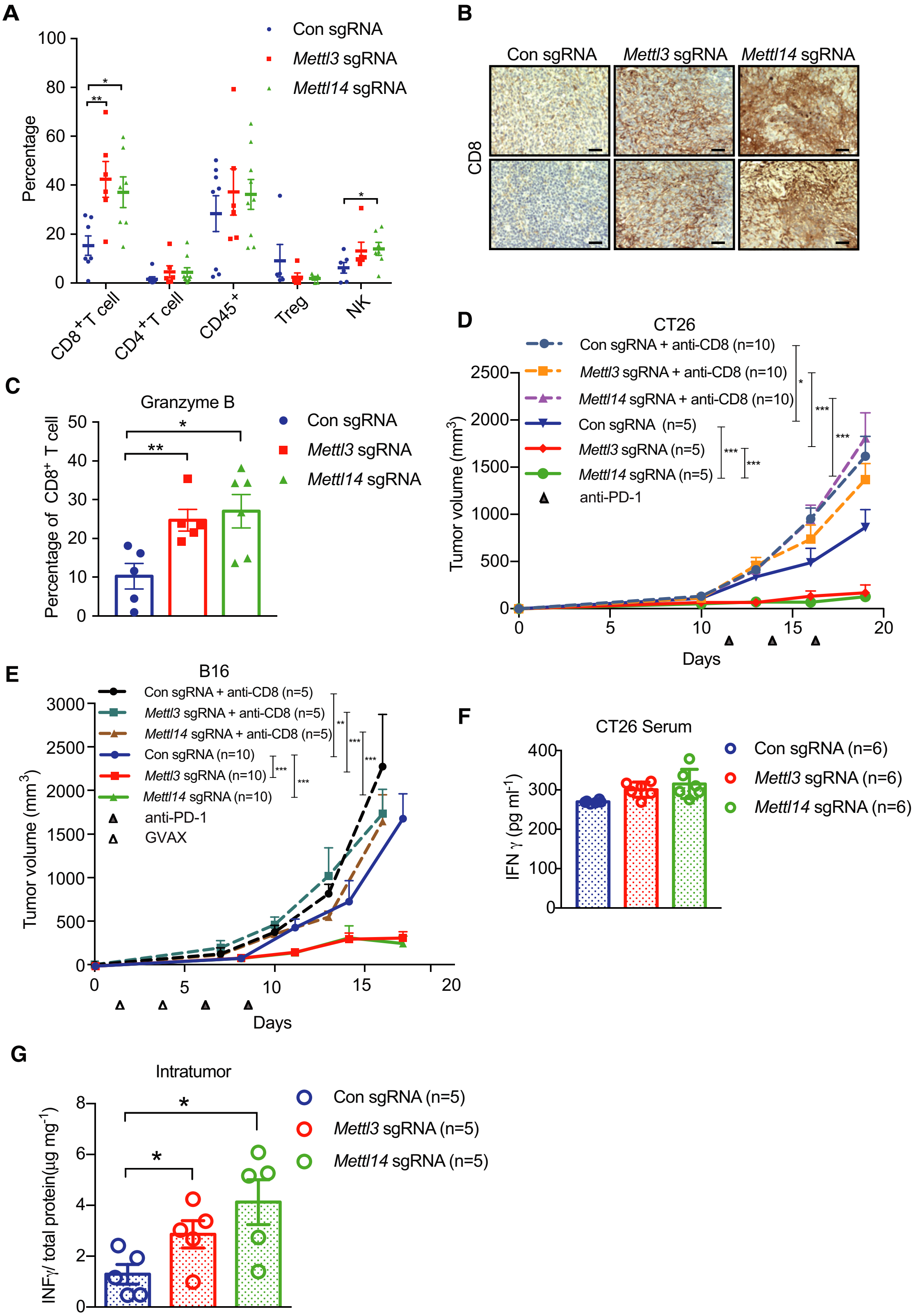
A
Con sgRNA
Mettl3 sgRNA
Mettl14 sgRNA
Percentage
CD8+T cell
CD4+T cell
CD45+
Treg
NK
B
Con sgRNA
Mettl3 sgRNA
Mettl14 sgRNA
CD8
C
Granzyme B
Percentage of CD8+ T cell
D
CT26
Con sgRNA + anti-CD8 (n=10)
Mettl3 sgRNA + anti-CD8 (n=10)
Mettl14 sgRNA + anti-CD8 (n=10)
Con sgRNA (n=5)
Mettl3 sgRNA (n=5)
Mettl14 sgRNA (n=5)
anti-PD-1
Tumor volume (mm3)
Days
E
B16
Con sgRNA + anti-CD8 (n=5)
Mettl3 sgRNA + anti-CD8 (n=5)
Mettl14 sgRNA + anti-CD8 (n=5)
Con sgRNA (n=10)
Mettl3 sgRNA (n=10)
Mettl14 sgRNA (n=10)
anti-PD-1
GVAX
Tumor volume (mm3)
Days
F
CT26 Serum
Con sgRNA (n=6)
Mettl3 sgRNA (n=6)
Mettl14 sgRNA (n=6)
IFN γ (pg ml-1)
G
Intratumor
Con sgRNA (n=5)
Mettl3 sgRNA (n=5)
Mettl14 sgRNA (n=5)
INFγ/ total protein(μg mg-1)

Figure 2.

Figure 2. Mettl3 or Mettl14 deficiency enhances tumor-infiltrating $CD8^+$ T cells and cytokine production.

A Percentage of tumor-infiltrating T cells, Treg, and NK cells were identified by flow cytometry from CT26 tumors as indicated. Each spot represents one mouse. $*P < 0.05$; $**P < 0.01$ by Student's *t*-tests.

B Representative images of CD8 by IHC staining. Tissue sections from BALB/c mice bearing the indicated knockout of genes with treatment of PD1 antibody. Scale bars, 50 μm.

C Percentage of granzyme B-expressing $CD8^+$ T cells from control and Mettl3- or Mettl14-deficient CT26 tumors. Each spot represents one mouse. $*P < 0.05$; $**P < 0.01$ by Student's *t*-tests.

D, E Mice bearing control and Mettl3 or Mettl14 null tumors were treated with CD8-depleting antibody and PD-1 antibody or PD-1/GVAX as indicated. Tumor volume was measured over time points. *n*, the numbers of mice. $*P < 0.05$; $**P < 0.01$; $***P < 0.001$ by Student's *t*-tests.

F, G IFN-γ production in serum (F) and intratumor (G) from BALB/c mice by ELISA. The results are representatives of at least three independent experiments. *n*, the numbers of mice. Data are mean ± SEM. $*P < 0.05$ by Student's *t*-tests.

(Fig EV5A and B). We next compared the tumor growth of these double knockout cells with tumors lacking Mettl3 or Mettl14 only under immunotherapy. Double loss of Mettl3/Stat1, Mettl3/Irf1, Mettl14/Stat1, and Mettl14/Irf1 reversed the observed effects on Mettl3- or Mettl14-deficient tumor growth (Figs 3I and EV5C–E). Moreover, the mice bearing these double knockout of Mettl3/Stat1, Mettl3/Irf1, Mettl14/Stat1, and Mettl14/Irf1 tumors have quite similar survival rate compared to control, whereas shortened survival than depleted Mettl3 or Mettl14 only (Fig EV5F). Thus, these data demonstrate that Stat1 and Irf1 are the main targets regulated by both Mettl3 and Mettl14.

Role of Mettl3 and Mettl14 in tumor cells response to IFN-γ

IFN-γ signaling is a key contributor in adaptive and acquired resistance to the checkpoint blockade therapeutic strategy and has impressive effects on antitumor immune responses (Sharma *et al*, 2017). We next investigated whether depletion of Mettl3 or Mettl14 could improve the response of tumor cells to IFN-γ. To this purpose, we first assessed whether IFN-γ has the effect on the growths of cells with knockout of Mettl3 or Mettl14. The results of cellular proliferation assay showed that Mettl3 or Mettl14 deficiency indeed sensitized CT26 cells to IFN-γ, and combined IFN-γ and TNFα-induced growth inhibition, but not TNFα alone, indicating that IFN-γ alone is sufficient to inhibit Mettl3 or Mettl14 deficient cell growth (Fig 4A). In line with this result, we also found that blocking of INFγ using anti-IFN-γ antibody in BALB/c mice partially reversed the inhibition of tumor growth by Mettl3 or Mettl14 depletion under immunotherapy, suggesting IFN-γ is responsible for the observed Mettl3 or Mettl14 loss-mediated suppression during immunotherapy (Fig 4B). Furthermore, transcriptional analysis of the Mettl3- or Mettl14-deficient and control CT26 cells with or without the stimulation of IFN-γ by qRT–PCR suggested that an increased expression of IFN-γ pathway genes including *Stat1* and *Irf1*, but no alteration of gene expression in unstimulated conditions (Fig 4C). Thus, the loss of Mettl3 or Mettl14 increased sensitivity to IFN-γ treatment. To determine whether the increased mRNA levels of *Stat1* and *Irf1*, in Mettl3 and Mettl14 null tumors, are a consequence of enhanced mRNA stability, we determined the half-life of these mRNAs. Control and Mettl3- or Mettl14-deficient cells with stimulation of IFN-γ were treated with actinomycin D for 0, 6, 12, and 24 h, and then, mRNA stability was monitored using qRT–PCR. This analysis revealed that Mettl3- and Mettl14-depleted cells contained more stabilized *Stat1* and *Irf1* mRNAs than control cells (Fig 4D and E), and this alternation is consistent with the observation of decreased m^6A enrichment in 3′UTR of *Stat1* and *Irf1* in Mettl3- or Mettl14-depleted tumors (Fig 3F).

To further explore how Mettl3 and Mettl14 regulate gene expression through its readers, since the downstream functions of m^6A rely on its readers-YTH family proteins, we generated knockout of Ythdf1-3 CT26 cells (Fig 4F) and then analyzed the expression of *Stat1* and *Irf1* in these Yths-depleted cells with or without treatment of IFN-γ by qRT–PCR. This analysis indicated that loss of Ythdf2 significantly increased the mRNA levels of *Stat1* and *Irf1* with stimulation of IFN-γ (Fig 4G). Accordingly, depletion of Ythdf2 partially reversed decreased mRNA stability of *Stat1* and *Irf1* caused by overexpression of Mettl3 or Mettl14 in cells with stimulation of IFN-γ and then treatment with actinomycin D for 0, 30, 60, and 90 min (Fig 4H–J). Altogether, these results support that Ythdf2-mediated mRNA stability controls *Stat1* and *Irf1* expression of Mettl3 and Mettl14 regulated genes.

METTL3 and METTL14 were negatively correlated with STAT1 in human pMMR-MSI-L CRC colon tissue

In agreement with our results of mouse model, we found a negative correlation between METTL3 or METTL14 and STAT1 in 59 patients with pMMR-MSI-L CRC tumors using immunohistochemistry (Fig 5A and B). Together, these results identify METTL3/14-STAT1 axis as a regulator of IFN-γ in pMMR-MSI-L CRC tumors and suggest that METTL3 and METTL14 inhibition could be a viable new strategy to sensitize these CRC tumors which are refractory to currently available immunotherapy treatments.

Discussion

Overall, our work demonstrates that RNA-modifying enzymes play a vital role in tumor survival during immunotherapy. Depletion of Mettl3 or Mettl14, core subunits of RNA methyltransferase, significantly slowed tumor growth and prolonged the survival in mouse bearing CT26 colorectal carcinoma and B16 melanoma with anti-PD1 or anti-PD1/GVAX treatments, respectively. Outside tumor cells, the elevation of $CD8^+$ T cells in both Mettl3 and Mettl14 null tumors and NK cells in Mettl14 null tumors, accompanied by the increased production of cytokines and chemokines including IFN-γ, Cxcl9, and Cxcl10 were detected, demonstrating the immune system and tumor microenvironment were altered under the abolishment of tumor m^6A mRNA transferases. Inside tumor cells, the changes of the transcriptome profile in methyltransferase-depleted tumor showed the activation of IFN-γ signaling was pivotal to re-sensitize tumor cells to immunotherapy. Epitranscriptome analysis indicated the loss of m^{6}A modification on the transcripts in IFN-γ-*Stat1*-*Irf1* axis contributed to their stabilization mediated by m^{6}A reader Ythdf2 thereby account for the upregulation of IFN-γ signaling and the change of tumor microenvironment. Furthermore, the depletion of Mettl3 or Mettl14 increased sensitivity to IFN-γ in tumor cells

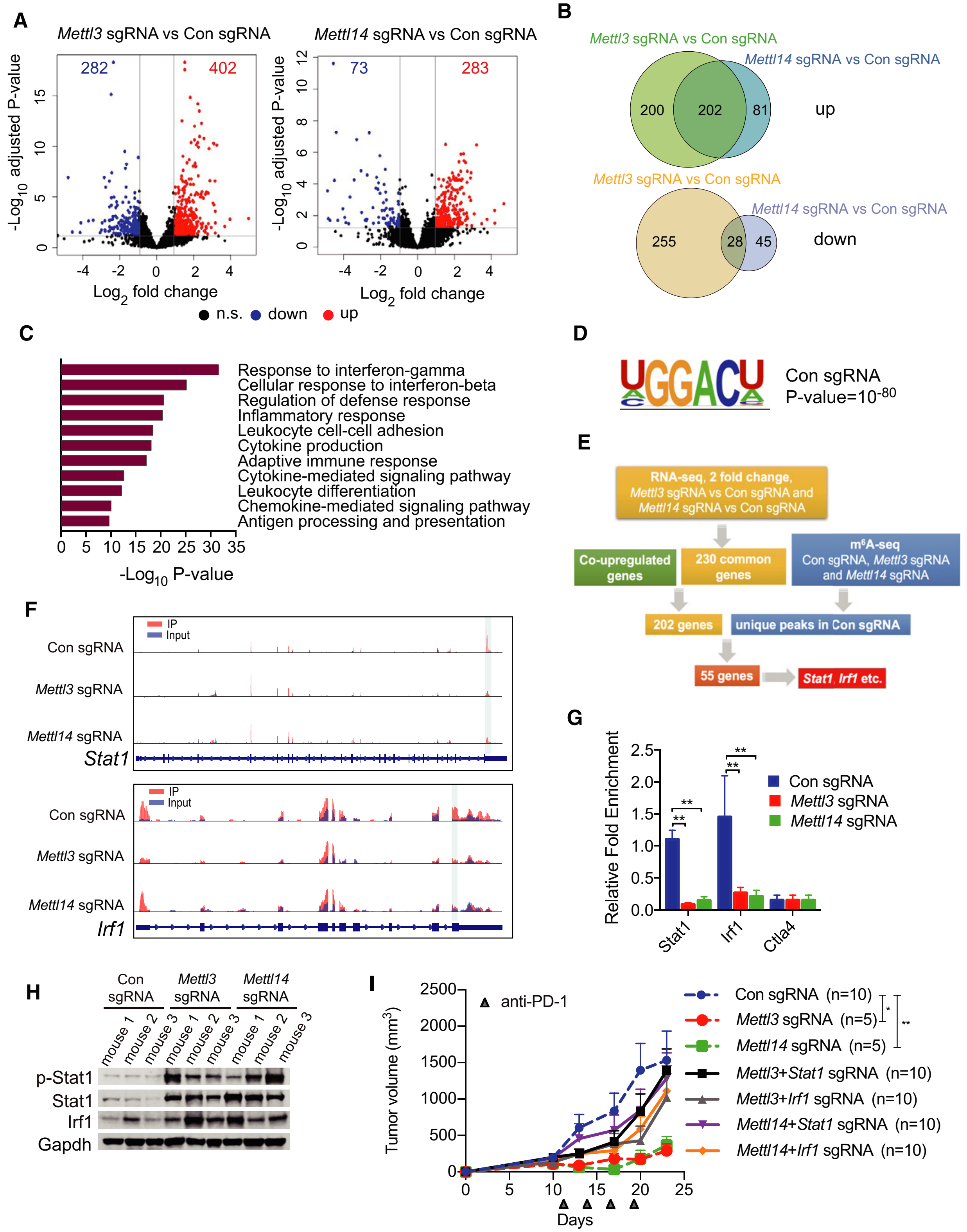

Figure 3.

Figure 3. Identification of target genes of Mettl3 and Mettl14 by RNA-seq and m^{6}A-seq.

A Volcano plot of differentially expressed genes obtained by DESeq2 analysis in Mettl3 or Mettl14 null tumors compared to control tumors. Significantly upregulated or downregulated genes are plotted in red and blue points, respectively. *n.s*, non-significant.

B Venn diagrams showing 202 significantly co-upregulated genes and 28 significantly co-downregulated genes in the indicated tumors.

C Meta-enrichment analysis summary for 202 significantly co-upregulated genes as indicated in (C).

D Consensus m^{6}A motifs and *P* value identified by HOMER from two biological replicates, Student's *t*-tests.

E Schematic workflow for analysis of Mettl3 and Mettl14 downstream genes and identified genes or peaks number.

F Representative genes with m^{6}A sites generated by integrative genomics viewer. Data are representative of duplicates with similar results. Red represents reads coverage of IP sample and blue represents reads coverage of input sample. Rectangular cyan shade represents the m^{6}A peaks located on transcripts.

G m^{6}A enrichment of *Stat1* and *Irf1* was examined by m^{6}A RIP-qPCR in control, Mettl3-, or Mettl14-depleted CT26 tumors as indicated. *Ctla4* functioned as a m^{6}A negative control (Wang *et al*, 2019). Data are mean ± SD. $^{**}P < 0.01$ by Student's *t*-tests.

H Immunoblots of p-Stat1 (phosphorylated), Stat1, and Irf1 were carried out in the indicated tumors in triplicate with Gapdh as a loading control.

I Tumor growth from CT26 cells with *Mettl3-*, *Mettl14-*, *Mettl3/Stat1-*, *Mettl3/Irf1-*, *Mettl14/Stat1-*, or *Mettl14/Irf1*-depleted genes and control under treatment of PD-1 antibody as indicated. *n*, the numbers of mice. Data are mean ± SEM of the indicated number of mice in each group. $^{*}P < 0.05$; $^{**}P < 0.01$ by Student's *t*-tests.

Source data are available online for this figure.

(Fig 5C). Lastly, based on the *in vivo* and *in vitro* observations, a negative correlation between METTL3/14 and STAT1 expression was also revealed in pMMR-MSS colorectal carcinoma patients to further substantiate the clinical value of our discovery.

It is worth noting that depletion of Mettl3 or Mettl14 alone did not affect tumor growth in mice, highlighting the unique role of m^{6}A in the tuning of certain pathways regulating immunotherapy. Previous studies reported that Mettl3 or Mettl14 depletion alone was able to affect cell proliferation or tumor growth in leukemia (Barbieri *et al*, 2017; Vu *et al*, 2017; Weng *et al*, 2018), glioblastoma (Cui *et al*, 2017), and hepatocellular carcinoma (Ma *et al*, 2017; Chen *et al*, 2018). In this study, however, the effect of RNA m^{6}A modification machinery loss on tumors only emerged under immunotherapy. These findings highlight that the function of m^{6}A mRNA modification varies under different physiological context and the role it plays to help tumors undergo specific external stresses like that from the immune system.

IFN-γ-Stat1-Irf1 axis plays an essential role in the interaction between tumor and immune system. The protective role of IFN-γ against implanted, chemically induced, and spontaneous tumors have been recorded in numerous studies since the mid-1990s (Dunn *et al*, 2002). At the molecular level, our MeRIP-seq and RNA-seq revealed the suppression of m^{6}A on the 3′UTR of *Stat1* and *Irf1* mRNA coupled with the elevation of their abundance. Accordingly, we also observed increased mRNA expression of *Cxcl9*, *Cxcl10* and production of Cxcl9, and Cxcl10 in tumors. Given that the extracellular secretion of Cxcl9-mediated lymphocytic infiltration to the tumor and suppressed tumor growth (Gorbachev *et al*, 2007), and Cxcl10 level was positively correlated with the number of circulating lymphocytes (Sridharan *et al*, 2016). Thus, it is likely that the activation of these chemokine genes and the elevation of their level within the intratumor environment, discovered in this study, accounts for the increased CD8$^+$ TILs and intratumor IFN-γ level, explaining the tumor inhibition by PD-1 antibody treatment.

Interestingly, a recent study reported that the knockdown of FTO sensitized melanoma cells to IFN-γ through the increase of m^{6}A enrichment and consequently destabilization of transcripts encoded by melanoma promoting genes, including PD-1, CXCR4, and SOX10 (Yang *et al*, 2019). At a first glance, this may seem that there is a discrepancy about the role that m^{6}A modification machinery plays in tumor immunosurveillance that could be explained by the use of different experimental mouse model (Yang *et al*, 2019), but more importantly, our work on Mettl3/14 and the reported FTO findings (Yang *et al*, 2019) underscore the significance of epitranscriptomic regulation of molecular networks in response to certain stress conditions during tumorigenesis and tumor microenvironment altered by immunotherapy. Three recent reports further support the notion that the role of RNA modification machinery to regulate mechanism of gene expression is more complex that previously envisioned. (a) Changes in m^{6}A mRNA levels by knockdown of either METTL14 or ALKBH5 inhibited cancer growth and invasion (Panneerdoss *et al*, 2018). ALKBH5/METTL14 formed a positive feedback loop with RNA stability factor HuR to regulate the stability of target transcripts. Further, hypoxia altered the level/activity of RNA modification machinery and expression of specific transcripts in cancer cells (Panneerdoss *et al*, 2018). (b) By developing and employing a new method, m^{6}A-Crosslinking-Exonuclease-sequencing (m^{6}ACE-seq), to map transcriptome-wide m^{6}A and m^{6}Am at quantitative single-base-resolution, Goh and colleagues discovered that both ALKBH5 and FTO maintained their regulated sites in an unmethylated steady-state (Koh *et al*, 2019). (c). The role of ALKBH5 in enhancing anti-PD-1 immunotherapy involves regulation of lactate content in the tumor microenvironment and the composition of tumor-infiltrating Treg and myeloid-derived suppressor cells (Li *et al*, 2020). Remarkably, ALKBH5 inhibition by a small molecule resulted in a similar phenotype and sensitized tumors to immunotherapy, indicating future translational potential of targeting m^{6}A regulating machinery in cancers (Li *et al*, 2020). However, these studies do not exclude the possibility that specific RNA modifications are written and erased under various stress conditions by translocation of enzymes. Therefore, dynamic imbalance of m^{6}A modification machinery location and function may affect the tumor progression and immunotherapy responses.

Despite the success of immunotherapy in the past decade, pMMR-MSI-L subtype colorectal cancer, the vast majority of CRC patients carried, failed to benefit from any immunotherapy alone (Ganesh *et al*, 2019). The lack of recruitment of immune cell to the tumor seems the primary reason since microsatellite instability-high (pMMR-MSI-H) colorectal cancer (Llosa *et al*, 2015), another subtype of CRC that responds well to immunotherapy, is featured by an interferon-rich microenvironment and heavily infiltrated immune cells like CD8$^+$ TILs, CD4$^+_{(Th1)}$ TILs, and macrophages

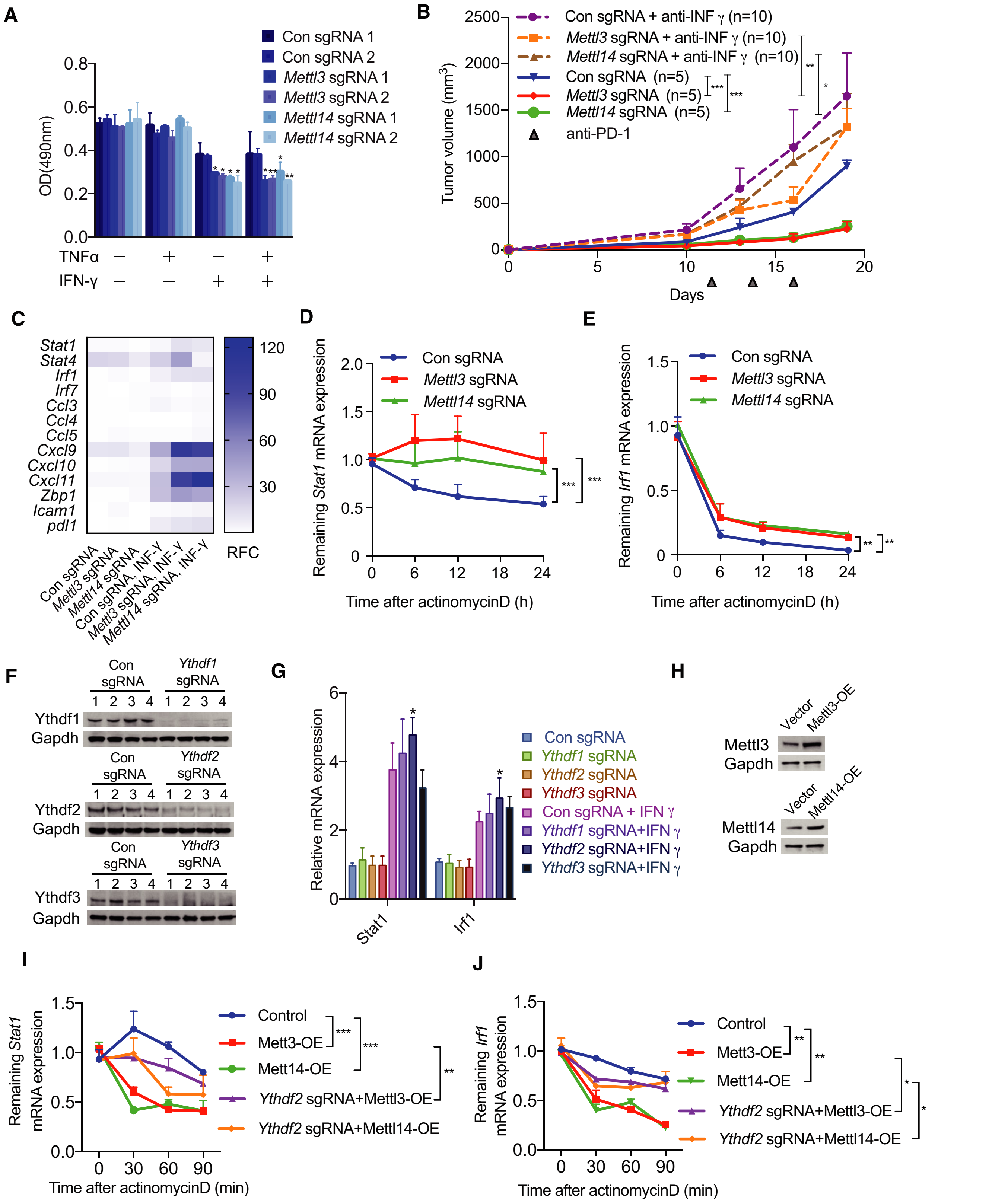
A
Con sgRNA 1
Con sgRNA 2
Mettl3 sgRNA 1
Mettl3 sgRNA 2
Mettl14 sgRNA 1
Mettl14 sgRNA 2
OD(490nm)
TNFα
IFN-γ
B
Con sgRNA + anti-INF γ (n=10)
Mettl3 sgRNA + anti-INF γ (n=10)
Mettl14 sgRNA + anti-INF γ (n=10)
Con sgRNA (n=5)
Mettl3 sgRNA (n=5)
Mettl14 sgRNA (n=5)
anti-PD-1
Tumor volume (mm3)
Days
C
Stat1
Stat4
Irf1
Irf7
Ccl3
Ccl4
Ccl5
Cxcl9
Cxcl10
Cxcl11
Zbp1
Icam1
pdl1
RFC
Con sgRNA
Mettl3 sgRNA
Mettl14 sgRNA
Con sgRNA, INF-γ
Mettl3 sgRNA, INF-γ
Mettl14 sgRNA, INF-γ
D
Con sgRNA
Mettl3 sgRNA
Mettl14 sgRNA
Remaining Stat1 mRNA expression
Time after actinomycinD (h)
E
Remaining Irf1 mRNA expression
Time after actinomycinD (h)
F
Con sgRNA
Ythdf1 sgRNA
Ythdf1
Gapdh
Ythdf2 sgRNA
Ythdf2
Ythdf3 sgRNA
Ythdf3
G
Relative mRNA expression
Con sgRNA
Ythdf1 sgRNA
Ythdf2 sgRNA
Ythdf3 sgRNA
Con sgRNA + IFN γ
Ythdf1 sgRNA+IFN γ
Ythdf2 sgRNA+IFN γ
Ythdf3 sgRNA+IFN γ
Stat1
Irf1
H
Vector
Mettl3-OE
Mettl3
Gapdh
Mettl14-OE
Mettl14
I
Control
Mett3-OE
Mett14-OE
Ythdf2 sgRNA+Mettl3-OE
Ythdf2 sgRNA+Mettl14-OE
Remaining Stat1 mRNA expression
Time after actinomycinD (min)
J
Remaining Irf1 mRNA expression
Time after actinomycinD (min)

Figure 4.

Figure 4. Tumor cells with knockout of Mettl3 or Mettl14 exhibit enhanced response to IFNγ.

A Cellular proliferation analysis of Mettl3- or Mettl14-depleted and control CT26 cells treated with indicated combinations of cytokines for 48 h. The mean ± SD of three replicates is shown. $^*P < 0.05$; $^{**}P < 0.01$ by Student's *t*-tests.

B BALB/c mice bearing Mettl3- or Mettl14-deficient and control tumors were treated with IFNγ-blocking antibody and PD-1 antibody as indicated. Tumor size was measured over time. *n*, the numbers of mice. Data are mean ± SEM of the indicated number of mice. $^*P < 0.05$; $^{**}P < 0.01$; $^{***}P < 0.001$ by Student's *t*-tests.

C Quantitative RT–PCR was performed to identify transcriptional changes of the IFN-γ response gene expression ($n = 3$). Data are shown as the relative fold change (RFC, color coded bar).

D, E mRNA stability of *Stat1* and *Irf1* were measured by qRT–PCR in tumor cells treated with IFN-γ and actinomycin D. Mean ± SD of $n = 3$. $^{**}P < 0.01$; $^{***}P < 0.001$ by Student's *t*-tests.

F Validation the effect of knockout of Ythdf1-3 using Western blotting, Gapdh served as a loading control.

G qPCR analysis of *Stat1* and *Irf1*'s expression in the indicated depletion of CT26 cells with/without stimulation of IFN-γ. Mean ± SD of $n = 3$. $^*P < 0.05$ by Student's *t*-tests.

H Western blot analysis of Mettl3 and Mettl14 in overexpressed CT26 cells. Gapdh served as a loading control for each.

I, J qPCR analysis of the mRNA stability of *Stat1* and *Irf1* in the indicated CT26 cells treated with IFN-γ and actinomycin D. Mean ± SD of $n = 3$. $^*P < 0.05$; $^{**}P < 0.01$; $^{***}P < 0.001$ by Student's *t*-tests.

Source data are available online for this figure.

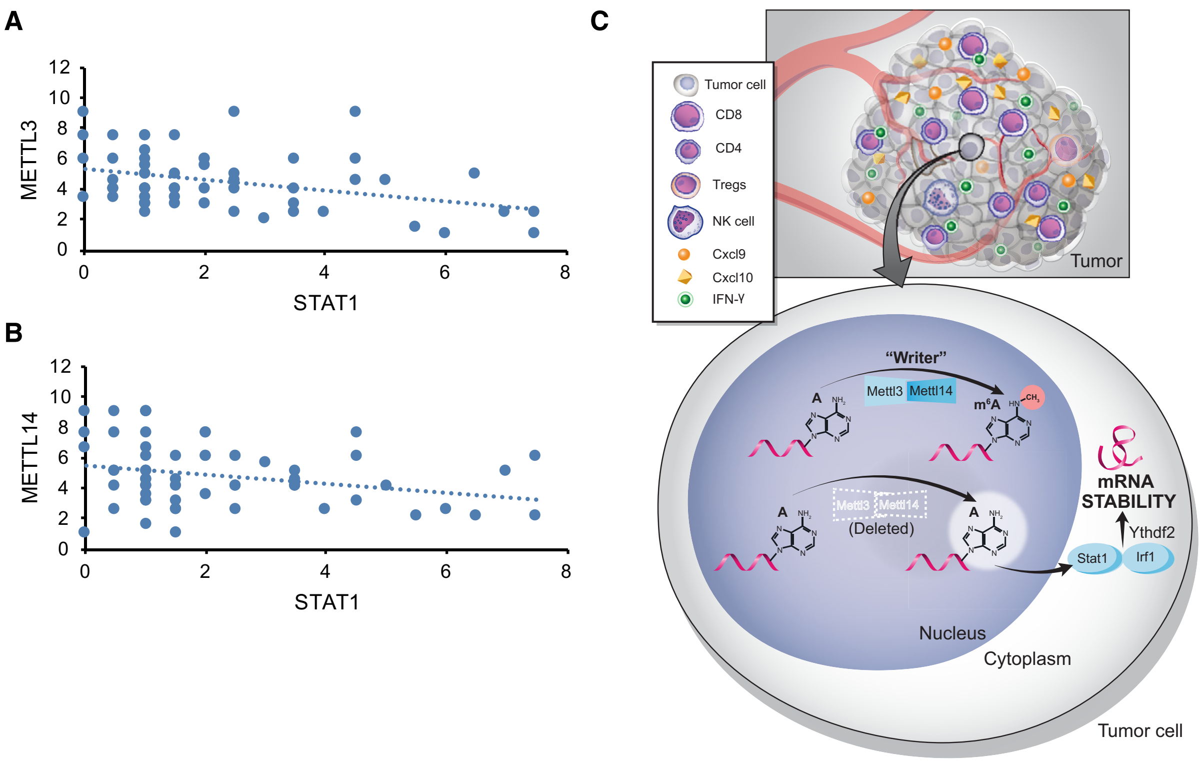

Figure 5. The negative correlation of METTL3, METTL14, and STAT1 in human pMMR-MSI-L CRC colon tissue.

A, B The protein level of STAT1 was negatively correlated with METTL3 and METTL14 in human pMMR-MSI-L CRC colon tissues ($r^2 = -3.2477$ for METTL3, $r^2 = -2.7491$ for METTL14). Each dot represents one tumor tissue.

C Schematic showing the functional and molecular mechanisms of Mettl3 and Mettl14 in antitumor immunotherapy.

(Deschoolmeester *et al*, 2011). Our results revealed that suppression of m^{6}A modification sensitized tumors to immunotherapy by altering the tumor microenvironment and recruitment of CD8$^+$ TILs. Notably, the growth inhibitory effects in Mettl3/14-depleted tumors we observed in the study were comparable to that of multiple combinatorial immunotherapy regimens (anti-PD-1+anti-CTLA-4). Thus, it is exciting to imagine the possibility that our study opens doors to combine immunotherapy with newly developed methyltransferase inhibitors for CRC therapy.

Taken together, we found the suppression of m^{6}A modification enhanced response to immunotherapy in colorectal carcinoma and melanoma. This sensitization effect in CRC tumors is mediated by the elevated *Stat1* and *Irf1* expression whose mRNA transcripts were stabilized by the decreased m^{6}A enrichment. This study demonstrates the essential role of m^{6}A writer in the maintenance of tumor surveillance to immunotherapy. The inhibition of m^{6}A writers also provides the opportunity to overcome the barrier in the pMMR-MSI-L colorectal cancer immunotherapy.

Materials and Methods

All studies were conducted in accordance with approved IRB protocols by the University of California, San Diego. All animal work was approved by the Institutional Review Board at the University of California, San Diego, and was performed in accordance with Institutional Animal Care and Use Committee guidelines.

Cell culture and viral infection

CT26 (CRL-2638; murine colon carcinoma) and B16F10 (CRL-6475; murine melanoma) were all purchased from ATCC. B16-GM-CSF cell line was a kind gift from Drs. Glenn Dranoff and Michael Dougan (Dana-Farber/Harvard Cancer Center). These cell lines were cultured in DMEM, RPMI (Gibco) supplemented with 10% fetal bovine serum (Gibco) at 37°C in 5% CO_2 incubators. HEK293FT cells were resuspended in DMEM and co-transfected with CRISPR V2 backbones with the indicated sgRNA, and packaging plasmids psPAX2, and pMD2.G in 10 cm dish using Lipofectamine (Life Technologies, 11668027) in Opti-MEM medium (Gibco). The medium was replaced with fresh completed DMEM after 4–6 h. The supernatant was harvested after 48 h and then infect cells by spin transduction. Finally, cells were selected by puromycin (Alfa Aesar, Thermo Fisher Scientific) or blasticidin (Alfa Aesar, Thermo Fisher Scientific). SgRNA used in this work was as follows: *Mettl3*-sgRNA1: TAGGCACGGGACTATC ACTACACCG; *Mettl3*-sgRNA2: TCAGGTGA TTACCGTAGAGA; *Mettl3*-sgRNA3: AGGTAGCAGGGACCATCGCA; *Mettl3*-sgRNA4: CTGAAGTGCAGCTTGCGACA; *Mettl14*-sgRNA1: GT CCAGTGTCTACAAAATGT; *Mettl14*-sgRNA2: CACTGAACTACTTA-CATGGG; *Mettl14*-sgRNA3: ATCAACTTACTACTCTCCCA; *Mettl14*-sgRNA4: GCTGGACCTGGGATGATGTA. *Ythdf1*-sgRNA1: AGCAGC-CACTTCAACCCCGC; *Ythdf1*-sgRNA2: TGAACACGGCAACAAGCG CC; *Ythdf1*-sgRNA3: GACTTTGAGCCCTACCTTTC; *Ythdf1*-sgRNA4: ACAAAAGGACAAGATAATAA. *Ythdf2*-sgRNA1: CGAACCTTACTT-GAGCCCAC; *Ythdf2*-sgRNA2: GCCGCCTATCGTTCCATGAA; *Ythdf2*-sgRNA3: TCGCAGAGACCAAAAGGTCA; *Ythdf2*-sgRNA4: AGATTC-CAGTCGAAATCTTT. *Ythdf3*-sgRNA1: TGAGCATGGTAATAAGCGT T; *Ythdf3*-sgRNA2: AAGCCGGTTCCCCTATTCCG; *Ythdf3*-sgRNA3: AAGAATGTCAGCCACTAGCG; *Ythdf3*-sgRNA4: CTTAAGTAGCCA-GACAAATC.

Immunoblotting

Proteins from cells or fresh mice tumors were extracted using RIPA lysis buffer by homogenization followed by centrifugation to remove insoluble material and clarified supernatant was measured using BCA protein assay kit (Bio-Rad). Subsequently, 50–150 μg of protein was resolved by NuPAGE Bis-Tris or 10% Tris-Glycine gels and transferred to PVDF membranes (Bio-Rad). Membranes were blocked in 5% milk TBST buffer and then incubated with the indicated antibodies including Mettl3 (Abcam, ab195352), Mettl14 (Fisher Scientific, ABE1338MI), Gapdh (PROTEINTECH GROUP, HRP-60004), Stat1 (PROTEINTECH GROUP, 10144-2-AP), p-Stat1 (Cell Signaling Technology), Irf1 (PROTEINTECH GROUP, 11335-1-AP), Ythdf1 (PROTEINTECH GROUP, 17479-1-AP), Ythdf2 (PROTEINTECH GROUP, 24744-1-AP), and Ythdf3 (Sigma-Aldrich, Inc., SAB2108258) overnight at 4°C. After being washed, membranes were incubated with HRP-conjugated secondary antibodies at 25°C for 1 h and visualized on autoradiography film (Genesee Scientific Inc, 30-100) using the enhanced chemiluminescence (ECL) detection system (Thermo Scientific).

Animal models

BALB/c and C57BL/6J mice (6–8 week) used for study were purchased from The Jackson Laboratory. 2×10^6 CT26 cells with knockout of Mettl3, Mettl14, Mettl3/Stat1, Mettl3/Irf1, Mettl14/Stat1, or Mettl14/Irf1 and control were suspended in 200 μl of PBS/Matrigel (Corning) (1:1) and then subcutaneously inoculated into flank of each mouse. BALB/c mice bearing CT26 tumors were injected intraperitoneally (i.p.) with 200 μg (10 mg/kg) of anti-CTLA-4 (Bio X Cell, mCD152) and/or anti-PD1 (Bio X Cell, clone 29F.1A12) and IgG (Bio X Cell, clone 2A3, BE0089) antibodies on days 11, 14, 17, 20, and 23 as recommended. (Kim *et al*, 2014) For the *in vivo* CD8 depletion study, CT26 tumor-bearing mice were additionally treated i.p. with 200 μg (10 mg/kg) of anti-CD8 antibody (Bio X Cell, clone YTS169.4) twice a week starting on day 8 and also injected i.p. with 200 μg (10 mg/kg) of anti-PD1 antibody as indicated. For the *in vivo* IFN-γ blocking assay, BALB/c mice bearing the indicated tumors were treated i.p. with 200 μg (10 mg/kg) of anti-IFN-γ antibody (Bio X Cell, Clone: XMG1.2) every 2 days starting on day 7 and also injected i.p. with 200 μg (10 mg/kg) of anti-PD1 antibody as indicated. 0.5×10^6 B16 cells with knockout of Mettl3, Mettl14, and control were implanted into the left flank, and 1×10^6 irradiated (100 Gy) B16-GM-CSF cells (GVAX) were injected into the right flank of each C57BL/6J mouse on days 1 and 4. B16 tumor-bearing mice were given a dose of 200 μg (10 mg/kg) of anti-PD1 antibody i.p. on days 6 and 9. For the *in vivo* depletion study, B16 tumor-bearing mice were treated i.p. with 200 μg (10 mg/kg) of anti-CD8 antibody (Bio X Cell, clone YTS169.4) twice a week starting on day 3 and also injected i.p. with 200 μg (10 mg/kg) of anti-PD1 antibody and GVAX were injected into the right flank as indicated. Tumor volumes were calculated according to the formula: volume (mm^3) = (longer diameter × shorter diameter^2)/2. Mice were monitored every 2 days as indicated. All animal studies were approved by the Institutional Animal Care and Use Committee of University of California, San Diego.

Flow cytometry analysis of tumor cells

Tumors with knockout of Mettl3, Mettl14, and control were collected from mice, weighted, mechanically diced, and then digested with 2 mg/ml collagenase P (Sigma-Aldrich) and 50 μg/ml DNase I (Sigma-Aldrich) at 37°C for 30 min. Then, these samples were filtered through 70-μm cell strainers and washed by cell staining buffer (BioLegend). The red blood cells were lysed with lysis buffer (BioLegend, 420301). After counting viable cells and these cells were blocked with TruStain FcX (anti-mouse CD16/32) antibody (BioLegend) and then incubated with Zombie Aqua Live/Dead fixable dye (BioLegend, 423102). Subsequently, specific antibodies recognized cell surface markers were stained. The intracellular staining procedures followed by the BioLegend protocol as recommended. Briefly, cells were fixed with fixation buffer (BioLegend, 420801), permeabilized, and stained with predetermined optimum combination of antibodies. Meanwhile, BD Compensation Beads (BD Biosciences, 552845) were used to optimize fluorescence compensation settings for multicolor flow cytometric analysis. Information about all the antibodies used in the flow cytometry analysis is provided below. CD45 (clone 30-F11), CD3ε (clone 145-2C11), CD4 (clone RM4-5), CD8 (clone 53-6.7), NK1.1(clone PK136), FoxP3 (clone MF-14), granzyme B (clone QA16A02), and all the antibodies were purchased from BioLegend.

Production of cytokine/chemokine analysis

Intratumoral cytokine extraction from freshly harvested CT26 tumors and serum samples were prepared as described previously (Amsen *et al*, 2009; Veinalde *et al*, 2017). The productions of IFN-γ, Cxcl9, and Cxcl10 were measured using IFN-γ Mouse ELISA Kit (Invitrogen, 88-7314-22), mouse CXCL9 ELISA Kit (Fisher Scientific, EMCXCL9), and mouse CXCL10 ELISA Kit (Fisher Scientific, EMCXCL10) according to the manufacturer's instructions, respectively.

RNA isolation and quantitative real-time PCR

Total RNA was extracted from fresh tumors using Direct-zol RNA MiniPrep Kit (Zymo Research, 11-331) and RNA extraction form cultured cells using Quick-RNA Miniprep Kit (Zymo Research, R1055) following the manufacturer's instructions. Gene expression was analyzed as previously described (Mu *et al*, 2018). cDNA was generated using the iScript Reverse Transcription Synthesis Kit (Bio-Rad, 1708841) and quantitative real-time PCR was used SsoAdvanced Universal SYBR Green PCR SuperMix (Bio-Rad, 1725270). All primers used for qPCR are listed in Table EV1.

RNA-Seq

Total RNA was isolated from CT26 tumors with knockout of Mettl3, Mettl14, and control (five mice tumors for biological replicates in each group). RNA-seq library preparation and sequencing were performed at the IGM Genomics Center, UCSD using Illumina HiSeq 4000. For the analysis, single-end reads were trimmed by cutadapt (v1.18) then mapped to mouse genome (mm10) using HISAT2 (v2.1.0). Transcripts were quantified by HTSeq (0.11.2), and differential expressed genes (DEGs) were then determined by DESeq2.

MeRIP-Seq and MeRIP-qPCR

mRNA was isolated from tumors using RiboMinus Transcriptome Isolation Kit (life technology, K1500-02) followed by the procedures as recommended. Purified mRNA samples were fragmented to 100–200 nucleotides with Fragmentation Reagents Kit (Invitrogen, AM8740) according to the manufacturer's protocol. 10% of total fragmented RNA was reserved as an input sample and the rest of fragmented RNA was further used for m^6A immunoprecipitation with the anti-N6-methyladenosine (m^6A) antibody (abcam, ab151230) in 500 μl IP binding buffer (150 mM NaCl, 10 mM Tris–HCl, pH 7.5, 0.1% NP-40) with RNase inhibitor at 4°C for 2 h and then adding the washed protein A/G magnetic beads (NEB) by IP binding buffer to the RNA-antibody immunoprecipitation mixture to rotate at 4°C for 2 h. The collected magnetic beads were washed twice in IP binding buffer, twice in low salt reaction buffer (50 mM NaCl, 10 mM Tris–HCl, pH 7.5, 0.1% NP-40) and twice in high salt reaction buffer (500 mM NaCl, 10 mM Tris–HCl, pH 7.5, 0.1% NP-40). The bound RNA was eluted from beads by adding 30 μl RLT buffer (QIAGEN) and incubated for 5 min at 25°C. Lastly, the eluted RNA was purified by ethanol precipitation and prepared for library generation using a TruSeq mRNA library preparation kit (Illumina). Sequencing was performed at IGM Genomics core, UCSD on an Illumina HiSeq4000 machine. Detection for enriched peaks in m^6A immunoprecipitation samples was performed by model-based analysis of ChIP-seq (MACS2) algorithm (v2.1.0), peaks were detected if their FDR was < 5% and fold enrichment was higher than 1. High-confidence peaks in both biological replicate samples were found by BEDtools *intersect* function. *De novo* motif search was performed by HOMER (v4.10). For m^6A-MeRIP-qPCR, we adopted the same protocol above, m^6A enrichment was determined by qPCR analysis with indicated primers on LightCycler 480 (Roche Diagnostics). Ctla4 without m^6A-modified transcript was used as negative control. (Wang *et al*, 2019) All primers used for MeRIP-qPCR are listed in Table EV1.

Dot-blot assays

mRNA from fresh tumors was isolated using Magnetic mRNA Isolation Kit (New England Biolabs, S1550S) and then denatured at 95°C for 3 min, followed by chilling on ice. Quantified mRNA was spotted on an Amersham Hybond-N^+ membrane (GE Healthcare, RPN3050B) and crosslinked to the membrane with UV radiation. The membrane was blocked in 5% of non-fat milk PBST buffer and then incubated with anti-m^6A antibody (1: 2,000; abcam) overnight at 4°C. After incubating with HRP-conjugated secondary antibodies, the membrane was visualized by SuperSignal West Femto Maximum Sensitivity Substrate (Thermo Fisher Scientific).

In vitro cytokines stimulation

Mettl3- or Mettl14-deficient CT26 cells and control cells were cultured in 12-well plates in RPMI/10% FBS with the indicated combinations of cytokines: TNFα (10 ng/ml, PeproTech) and IFN-γ (100 ng/ml, BioLegend). Cells were further analyzed after 60 h.

Cell proliferation assays

A total of 2000 cells were plated in the 96-well plate, cells with the indicated sgRNA were determined by CellTiter AQueous One Solution Cell Proliferation Assay kit (Promega, G3580) following the manufacturer's instructions. Briefly, adding 20 μl of CellTiter Reagent into each well of the 96-well plate containing the cells. Incubating the plate at 37°C in 5% CO_2 incubators for 1–2 h, and then record the absorbance at 490 nm.

mRNA stability measurements

An mRNA stability measurement assay was performed as previously reported.(Wei *et al*, 2018a; Wang *et al*, 2019). Briefly, CT26 cells with knockout of Mettl3, Mettl14, and control or overexpression of Mettl3, Mettl14, and a combination with depletion of Ythdf2 were stimulated with IFN-γ. After 48 h, 5 μg/ml of Actinomycin D (Alfa Aesar, AAJ67160XF) was added for 0, 6, 12, and 24 h or 0, 30, 60, 90 min as indicated and then these cells were collected.

Subsequently, mRNA levels were quantified by RT–qPCR with gene-specific qPCR primers (Table EV1).

Immunohistochemistry

Human colon cancer tissues used in this study were obtained from US Biomax.inc. The staining analysis followed the previous description. (Mu *et al*, 2018) Briefly, slides of paraffin-embedded from human and mouse tissue were deparaffinized in xylene and rehydrated in graded ethanol (5 min in 100%, 5 min in 95%, and 5 min in 75%) and then washed by PBS containing 0.3% Triton X-100 (Sigma-Aldrich) (PBST) for three times. Sections were pretreated with antigen retrieval with Tris/EDTA buffer pH 9.0, rinsed three times with PBST, incubated with 3% H_2O_2 in PBS at 37°C for 10 min. After blocking with 5% goat serum (Cell Signaling Technology, 5425S) in PBST for 1 h, tissue slides were incubated at 4°C overnight with primary antibodies as follows: Mettl3 (Abcam, ab195352), Mettl14 (Fisher Scientific, ABE1338MI), Stat1(PROTEINTECH GROUP, 10144-2-AP), MSH2 (PROTEINTECH GROUP,15520-1-AP), Ki-67 (Cell Signaling Technology, 12202T), and CD8 (Cell Signaling Technology, 98941T). Then, the sections were washed by PBST for five times, incubated with biotinylated goat anti-rabbit IgG (Vector laboratories, BA-1000) at 25°C for 1 h and treated with AEC substrate kit (Vector laboratories, SK-4205) for 5 min and then counterstained with hematoxylin. Finally, all the mouse and human colon tissue slides were imaged. For the human colon cancer slides, images were obtained and semiquantitative evaluation of staining was scored as follows: score = percentage of malignant cells staining positive (0 < 10%; 1, 10–25%; 2, 25–50%; 3, > 50%) × mean stain intensity (0–3) as previously defined (Lin *et al*, 2014).

Statistical analysis

Results were analyzed using Prism 5.0 software (GraphPad) and presented as mean ± SEM (standard error) or mean ± SD (standard deviation) as indicated. P values were calculated using Student's t-tests and considered to be statistically significance at $P < 0.05$.

Data availability

The RNA-seq data and MeRIP-Seq data in this study were deposited at the Gene Expression Omnibus (GEO, https://www.ncbi.nlm.nih.gov/geo/) database with an accession number GSE142589 (related to Fig 3).

Expanded View for this article is available online.

Acknowledgements

We thank Drs. Glenn Dranoff and Michael Dougan for providing the B16 (GVAX) cells. We also thank Ye Wang (Peking University, Beijing, China) for help in RNA-seq and m^{6}A-seq data analysis, Dr. Kristen Jepsen of the Institute of Genomic Medicine at UCSD for help with the HTSeq, Dr. Neal Sekiya, and Ms. Tara Rambaldo at the Center for AIDS Research at UCSD for flow cytometry analysis, Dr. M. Valeria Estrada at the Biorepository and Tissue Technology Shared Resource at UC San Diego Moores Cancer Center for Histology and Immunohistochemistry, and members of the Rana laboratory for helpful discussions and advice. This publication includes data generated at the UC San Diego IGM Genomics Center utilizing an Illumina NovaSeq 6000 that was purchased with funding from a National Institutes of Health SIG grant (#S10 OD026929). This work was supported in part by grants from the National Institutes of Health (CA177322, DA039562, DA046171, and AI 125103).

Author contributions

LW designed and performed the experiments, analyzed the data, and wrote the manuscript; HH, KA, and YK performed the bioinformatics analyses; NL, RT, and JY performed experiments; TMR conceived, designed, and planned the project, and participated in experimental design, data analysis, data interpretation, and manuscript writing.

Conflict of interest

T.M.R. is a founder of ViRx Pharmaceuticals and has an equity interest in the company. The terms of this arrangement have been reviewed and approved by the University of California San Diego in accordance with its conflict of interest policies.

References

Alexandrov LB, Nik-Zainal S, Wedge DC, Aparicio SA, Behjati S, Biankin AV, Bignell GR, Bolli N, Borg A, Børresen-Dale A-L (2013) Signatures of mutational processes in human cancer. *Nature* 500: 415

Amsen D, de Visser KE, Town T (2009) Approaches to determine expression of inflammatory cytokines. In Inflammation and Cancer (Springer), pp. 107 – 142

Ayers M, Lunceford J, Nebozhyn M, Murphy E, Loboda A, Kaufman DR, Albright A, Cheng JD, Kang SP, Shankaran V *et al* (2017) IFN-gamma-related mRNA profile predicts clinical response to PD-1 blockade. *J Clin Invest* 127: 2930 – 2940

Barbieri I, Tzelepis K, Pandolfini L, Shi J, Millán-Zambrano G, Robson SC, Aspris D, Migliori V, Bannister AJ, Han N (2017) Promoter-bound METTL3 maintains myeloid leukaemia by m6A-dependent translation control. *Nature* 552: 126

Castro F, Cardoso AP, Gonçalves RM, Serre K, Oliveira MJ (2018) Interferon-gamma at the crossroads of tumor immune surveillance or evasion. *Front Immunol* 9: 847

Chen M, Wei L, Law CT, Tsang FHC, Shen J, Cheng CLH, Tsang LH, Ho DWH, Chiu DKC, Lee JMF (2018) RNA N6-methyladenosine methyltransferase-like 3 promotes liver cancer progression through YTHDF2-dependent posttranscriptional silencing of SOCS2. *Hepatology* 67: 2254 – 2270

Cui Q, Shi H, Ye P, Li L, Qu Q, Sun G, Sun G, Lu Z, Huang Y, Yang C-G (2017) m6A RNA methylation regulates the self-renewal and tumorigenesis of glioblastoma stem cells. *Cell Rep* 18: 2622 – 2634

Deng X, Su R, Weng H, Huang H, Li Z, Chen J (2018) RNA N6-methyladenosine modification in cancers: current status and perspectives. *Cell Res* 28: 507 – 517

Deschoolmeester V, Baay M, Lardon F, Pauwels P, Peeters M (2011) Immune cells in colorectal cancer: prognostic relevance and role of MSI. *Cancer Microenviron* 4: 377 – 392

Dominissini D, Moshitch-Moshkovitz S, Schwartz S, Salmon-Divon M, Ungar L, Osenberg S, Cesarkas K, Jacob-Hirsch J, Amariglio N, Kupiec M *et al* (2012) Topology of the human and mouse m6A RNA methylomes revealed by m6A-seq. *Nature* 485: 201 – 206

Dunn GP, Bruce AT, Ikeda H, Old LJ, Schreiber RD (2002) Cancer immunoediting: from immunosurveillance to tumor escape. *Nat Immunol* 3: 991

Ganesh K, Stadler ZK, Cercek A, Mendelsohn RB, Shia J, Segal NH, Diaz LA (2019) Immunotherapy in colorectal cancer: rationale, challenges and potential. *Nat Rev Gastroenterol Hepatol* 16: 361 – 375

Garcia-Diaz A, Shin DS, Moreno BH, Saco J, Escuin-Ordinas H, Rodriguez GA, Zaretsky JM, Sun L, Hugo W, Wang X (2017) Interferon receptor signaling pathways regulating PD-L1 and PD-L2 expression. *Cell Rep* 19: 1189 – 1201

Gorbachev AV, Kobayashi H, Kudo D, Tannenbaum CS, Finke JH, Shu S, Farber JM, Fairchild RL (2007) CXC chemokine ligand 9/monokine induced by IFN-γ production by tumor cells is critical for T cell-mediated suppression of cutaneous tumors. *J Immunol* 178: 2278 – 2286

Han D, Liu J, Chen C, Dong L, Liu Y, Chang R, Huang X, Liu Y, Wang J, Dougherty U (2019) Anti-tumour immunity controlled through mRNA m 6 A methylation and YTHDF1 in dendritic cells. *Nature* 566: 270

Honda K, Takaoka A, Taniguchi T (2006) Type I interferon gene induction by the interferon regulatory factor family of transcription factors. *Immunity* 25: 349 – 360

Hsu PJ, Zhu Y, Ma H, Guo Y, Shi X, Liu Y, Qi M, Lu Z, Shi H, Wang J (2017) Ythdc2 is an N6-methyladenosine binding protein that regulates mammalian spermatogenesis. *Cell Res* 27: 1115

Jaffrey SR, Kharas MG (2017) Emerging links between m(6)A and misregulated mRNA methylation in cancer. *Genome Med* 9: 2

Jenkins RW, Barbie DA, Flaherty KT (2018) Mechanisms of resistance to immune checkpoint inhibitors. *Br J Cancer* 118: 9

Jia G, Fu Y, Zhao X, Dai Q, Zheng G, Yang Y, Yi C, Lindahl T, Pan T, Yang Y-G (2011) N6-methyladenosine in nuclear RNA is a major substrate of the obesity-associated FTO. *Nat Chem Biol* 7: 885

Khalil DN, Smith EL, Brentjens RJ, Wolchok JD (2016) The future of cancer treatment: immunomodulation, CARs and combination immunotherapy. *Nat Rev Clin Oncol* 13: 273

Kim K, Skora AD, Li Z, Liu Q, Tam AJ, Blosser RL, Diaz LA, Papadopoulos N, Kinzler KW, Vogelstein B (2014) Eradication of metastatic mouse cancers resistant to immune checkpoint blockade by suppression of myeloid-derived cells. *Proc Natl Acad Sci USA* 111: 11774 – 11779

Koh CWQ, Goh YT, Goh WSS (2019) Atlas of quantitative single-base-resolution N6-methyl-adenine methylomes. *Nat Commun* 10: 5636

Kowanetz M, Zou W, Gettinger SN, Koeppen H, Kockx M, Schmid P, Kadel EE III, Wistuba I, Chaft J, Rizvi NA *et al* (2018) Differential regulation of PD-L1 expression by immune and tumor cells in NSCLC and the response to treatment with atezolizumab (anti-PD-L1). *Proc Natl Acad Sci USA* 115: E10119 – E10126

Le DT, Durham JN, Smith KN, Wang H, Bartlett BR, Aulakh LK, Lu S, Kemberling H, Wilt C, Luber BS *et al* (2017) Mismatch repair deficiency predicts response of solid tumors to PD-1 blockade. *Science* 357: 409 – 413

Li A, Chen Y-S, Ping X-L, Yang X, Xiao W, Yang Y, Sun H-Y, Zhu Q, Baidya P, Wang X (2017) Cytoplasmic m6A reader YTHDF3 promotes mRNA translation. *Cell Res* 27: 444

Li N, Kang Y, Wang L, Huff S, Tang R, Hui H, Agrawal K, Gonzalez GM, Wang Y, Patel SP *et al* (2020) ALKBH5 regulates anti-PD-1 therapy response by modulating lactate and suppressive immune cell accumulation in tumor microenvironment. *Proc Natl Acad Sci USA* 117: 20159 – 20170

Lichinchi G, Gao S, Saletore Y, Gonzalez GM, Bansal V, Wang Y, Mason CE, Rana TM (2016a) Dynamics of the human and viral m(6)A RNA methylomes during HIV-1 infection of T cells. *Nat Microbiol* 1: 16011

Lichinchi G, Zhao BS, Wu Y, Lu Z, Qin Y, He C, Rana TM (2016b) Dynamics of human and viral RNA methylation during zika virus infection. *Cell Host Microbe* 20: 666 – 673

Lichinchi G, Rana TM (2019) Profiling of N(6)-Methyladenosine in Zika Virus RNA and Host Cellular mRNA. *Methods Mol Biol* 1870: 209 – 218

Lichterfeld M, Xu GY, Waring MT, Mui SK, Johnston MN, Cohen D, Addo MM, Zaunders J, Alter G, Pae E (2004) HIV-1–specific cytotoxicity is preferentially mediated by a subset of CD8+ T cells producing both interferon-γ and tumor necrosis factor–α. *Blood* 104: 487 – 494

Lin Y, Zhang H, Liang J, Li K, Zhu W, Fu L, Wang F, Zheng X, Shi H, Wu S (2014) Identification and characterization of alphavirus M1 as a selective oncolytic virus targeting ZAP-defective human cancers. *Proc Natl Acad Sci USA* 111: E4504 – E4512

Liu J, Yue Y, Han D, Wang X, Fu Y, Zhang L, Jia G, Yu M, Lu Z, Deng X (2014) A METTL3–METTL14 complex mediates mammalian nuclear RNA N 6-adenosine methylation. *Nat Chem Biol* 10: 93

Liu J, Harada BT, He C (2019) Regulation of gene expression by N(6)-methyladenosine in cancer. *Trends Cell Biol* 29: 487 – 499

Llosa NJ, Cruise M, Tam A, Wicks EC, Hechenbleikner EM, Taube JM, Blosser RL, Fan H, Wang H, Luber BS (2015) The vigorous immune microenvironment of microsatellite instable colon cancer is balanced by multiple counter-inhibitory checkpoints. *Cancer Discov* 5: 43 – 51

Ma JZ, Yang F, Zhou CC, Liu F, Yuan JH, Wang F, Wang TT, Xu QG, Zhou WP, Sun SH (2017) METTL14 suppresses the metastatic potential of hepatocellular carcinoma by modulating N6−methyladenosine-dependent primary MicroRNA processing. *Hepatology* 65: 529 – 543

Mandal R, Samstein RM, Lee KW, Havel JJ, Wang H, Krishna C, Sabio EY, Makarov V, Kuo F, Blecua P *et al* (2019) Genetic diversity of tumors with mismatch repair deficiency influences anti-PD-1 immunotherapy response. *Science* 364: 485 – 491

Manguso RT, Pope HW, Zimmer MD, Brown FD, Yates KB, Miller BC, Collins NB, Bi K, LaFleur MW, Juneja V (2017) *In vivo* CRISPR screening identifies Ptpn2 as a cancer immunotherapy target. *Nature* 547: 413

Meyer KD, Saletore Y, Zumbo P, Elemento O, Mason CE, Jaffrey SR (2012) Comprehensive analysis of mRNA methylation reveals enrichment in 3′UTRs and near stop codons. *Cell* 149: 1635 – 1646

Meyer KD, Jaffrey SR (2017) Rethinking m(6)A readers, writers, and erasers. *Annu Rev Cell Dev Biol* 33: 319 – 342

Mu Y, Yan X, Li D, Zhao D, Wang L, Wang X, Gao D, Yang J, Zhang H, Li Y (2018) NUPR1 maintains autolysosomal efflux by activating SNAP25 transcription in cancer cells. *Autophagy* 14: 654 – 670

Nachtergaele S, He C (2018) Chemical modifications in the life of an mRNA transcript. *Annu Rev Genet* 52: 349 – 372

Paliard X, de Waal Malefijt R, de Vries JE, Spits H (1988) Interleukin-4 mediates CDS induction on human CD4+ T-cell clones. *Nature* 335: 642

Pandiyan P, Hegel JKE, Krueger M, Quandt D, Brunner-Weinzierl MC (2007) High IFN-γ production of individual CD8 T lymphocytes is controlled by CD152 (CTLA-4). *J Immunol* 178: 2132 – 2140

Panneerdoss S, Eedunuri VK, Yadav P, Timilsina S, Rajamanickam S, Viswanadhapalli S, Abdelfattah N, Onyeagucha BC, Cui X, Lai Z (2018) Cross-talk among writers, readers, and erasers of m6A regulates cancer growth and progression. *Sci Adv* 4: eaar8263

Pautz A, Art J, Hahn S, Nowag S, Voss C, Kleinert H (2010) Regulation of the expression of inducible nitric oxide synthase. *Nitric Oxide* 23: 75 – 93

Ping X-L, Sun B-F, Wang L, Xiao W, Yang X, Wang W-J, Adhikari S, Shi Y, Lv Y, Chen Y-S (2014) Mammalian WTAP is a regulatory subunit of the RNA N6-methyladenosine methyltransferase. *Cell Res* 24: 177

Ramana CV, Chatterjee-Kishore M, Nguyen H, Stark GR (2000) Complex roles of Stat1 in regulating gene expression. *Oncogene* 19: 2619

Ribas A, Wolchok JD (2018) Cancer immunotherapy using checkpoint blockade. *Science* 359: 1350 – 1355

Samstein RM, Lee CH, Shoushtari AN, Hellmann MD, Shen R, Janjigian YY, Barron DA, Zehir A, Jordan EJ, Omuro A *et al* (2019) Tumor mutational load predicts survival after immunotherapy across multiple cancer types. *Nat Genet* 51: 202 – 206

Schreiber RD, Old LJ, Smyth MJ (2011) Cancer immunoediting: integrating immunity's roles in cancer suppression and promotion. *Science* 331: 1565 – 1570

Sharma P, Allison JP (2015) The future of immune checkpoint therapy. *Science* 348: 56 – 61

Sharma P, Hu-Lieskovan S, Wargo JA, Ribas A (2017) Primary, adaptive, and acquired resistance to cancer immunotherapy. *Cell* 168: 707 – 723

Sridharan V, Margalit DN, Lynch SA, Severgnini M, Zhou J, Chau NG, Rabinowits G, Lorch JH, Hammerman PS, Hodi FS (2016) Definitive chemoradiation alters the immunologic landscape and immune checkpoints in head and neck cancer. *Br J Cancer* 115: 252

Tokunaga R, Zhang W, Naseem M, Puccini A, Berger MD, Soni S, McSkane M, Baba H, Lenz H-J (2018) CXCL9, CXCL10, CXCL11/CXCR3 axis for immune activation–a target for novel cancer therapy. *Cancer Treat Rev* 63: 40 – 47

Townsend SE, Allison JP (1993) Tumor rejection after direct costimulation of CD8+ T cells by B7-transfected melanoma cells. *Science* 259: 368 – 370

Veinalde R, Grossardt C, Hartmann L, Bourgeois-Daigneault M-C, Bell JC, Jäger D, von Kalle C, Ungerechts G, Engeland CE (2017) Oncolytic measles virus encoding interleukin-12 mediates potent antitumor effects through T cell activation. *Oncoimmunology* 6: e1285992

Vu LP, Pickering BF, Cheng Y, Zaccara S, Nguyen D, Minuesa G, Chou T, Chow A, Saletore Y, MacKay M (2017) The N6-methyladenosine (m6A)-forming enzyme METTL3 controls myeloid differentiation of normal hematopoietic and leukemia cells. *Nat Med* 23: 1369

Wang X, Lu Z, Gomez A, Hon GC, Yue Y, Han D, Fu Y, Parisien M, Dai Q, Jia G (2014) N6-methyladenosine-dependent regulation of messenger RNA stability. *Nature* 505: 117

Wang X, Zhao BS, Roundtree IA, Lu Z, Han D, Ma H, Weng X, Chen K, Shi H, He C (2015) N6-methyladenosine modulates messenger RNA translation efficiency. *Cell* 161: 1388 – 1399

Wang H, Hu X, Huang M, Liu J, Gu Y, Ma L, Zhou Q, Cao X (2019) Mettl3-mediated mRNA m6A methylation promotes dendritic cell activation. *Nat Commun* 10: 1898

Wei L-H, Song P, Wang Y, Lu Z, Tang Q, Yu Q, Xiao Y, Zhang X, Duan H-C, Jia G (2018a) The m6A reader ECT2 controls trichome morphology by affecting mRNA stability in *Arabidopsis*. *Plant Cell* 30: 968 – 985

Wei SC, Duffy CR, Allison JP (2018b) Fundamental mechanisms of immune checkpoint blockade therapy. *Cancer Discov* 8: 1069 – 1086

Weng H, Huang H, Wu H, Qin X, Zhao BS, Dong L, Shi H, Skibbe J, Shen C, Hu C (2018) METTL14 inhibits hematopoietic stem/progenitor differentiation and promotes leukemogenesis via mRNA m6A modification. *Cell Stem Cell* 22: 191 – 205 e199

Wu F, Cheng W, Zhao F, Tang M, Diao Y, Xu R (2019) Association of N6-methyladenosine with viruses and related diseases. *Virol J* 16: 133

Xiao W, Adhikari S, Dahal U, Chen Y-S, Hao Y-J, Sun B-F, Sun H-Y, Li A, Ping X-L, Lai W-Y (2016) Nuclear m6A reader YTHDC1 regulates mRNA splicing. *Mol Cell* 61: 507 – 519

Yang S, Wei J, Cui Y-H, Park G, Shah P, Deng Y, Aplin AE, Lu Z, Hwang S, He C (2019) m6A mRNA demethylase FTO regulates melanoma tumorigenicity and response to anti-PD-1 blockade. *Nat Commun* 10: 2782

Yue Y, Liu J, He C (2015) RNA N6-methyladenosine methylation in post-transcriptional gene expression regulation. *Genes Dev* 29: 1343 – 1355

Zenke K, Muroi M, Tanamoto KI (2018) IRF1 supports DNA binding of STAT1 by promoting its phosphorylation. *Immunol Cell Biol* 96: 1095 – 1103

Zheng G, Dahl JA, Niu Y, Fedorcsak P, Huang C-M, Li CJ, Vågbø CB, Shi Y, Wang W-L, Song S-H (2013) ALKBH5 is a mammalian RNA demethylase that impacts RNA metabolism and mouse fertility. *Mol Cell* 49: 18 – 29